SPECIAL ISSUE - MINI REVIEW

WILEY | Journal of RAMAN SPECTROSCOPY

Resonant broadband stimulated Raman scattering in myoglobin

C. Ferrante[1,2] | G. Batignani[1] | G. Fumero[1,3] | E. Pontecorvo[1] | A. Virga[1,2] |
L. C. Montemiglio[4] | G. Cerullo[5] | M. H. Vos[6] | T. Scopigno[1,2]

[1]Dipartimento di Fisica, Università di
Roma "La Sapienza", I-00185 Rome, Italy

[2]Istituto Italiano di Tecnologia, Center for
Life Nano Science at Sapienza, Roma,
I-00161, Italy

[3]Dipartimento di Scienze di Base e
Applicate per l'Ingegneria, Università di
Roma "La Sapienza", I-00185, Roma, Italy

[4]Dipartimento di Scienze Biochimiche
"Alessandro Rossi Fanelli",
Università di Roma "La Sapienza", I-00185
Rome, Italy

[5]IFN-CNR, Dipartimento di Fisica,
Politecnico di Milano, P.zza L. da Vinci 32
20133 Milan, Italy

[6]LOB, Ecole Polytechnique, CNRS,
INSERM, Université Paris-Saclay, 91128
Palaiseau Cedex, France

Correspondence
T. Scopigno, Dipartimento di
Fisica, Università di Roma "La
Sapienza", I-00185 Rome, Italy.
Email: tullio.scopigno@phys.uniroma1.it

Abstract

Spontaneous Raman is a well-established tool to probe molecular vibrations. Under resonant conditions, it is a largely used method for characterizing the structure of heme-proteins. In recent years, advances in pulsed laser sources allowed to explore vibrational features with complex techniques based on nonlinear optical interactions, among which is stimulated Raman scattering (SRS). Building on its combined spectral–temporal resolutions and high chemical sensitivities, SRS has been largely applied as a probe for ultrafast, time-resolved studies, as well as an imaging technique in biological systems. By using a frequency tunable, narrowband pump pulse jointly with a femtosecond white light continuum to initiate the SRS process, here we measure the Raman spectrum of a prototypical heme-protein, namely deoxy myoglobin, under two different electronic resonances. The SRS results are compared with the spontaneous Raman spectra, and the relative advantages, such as the capability of our experimental approach to provide an accurate mapping of Raman excitation profiles, are discussed.

KEYWORDS

chemical physics, heme-proteins, nonlinear optics, resonance Raman spectroscopy, stimulated Raman scattering

1 | INTRODUCTION

The study of molecular vibrations is pivotal for the understanding of physical and biochemical processes, allowing to extract structural and dynamical information. A powerful technique for this purpose is spontaneous Raman (SR), which is widely applied for the investigation of complex molecular systems and condensed matter. Large (up to 10^6 times) and mode specific enhancement of the vibrational response is achieved by tuning the Raman excitation wavelength to match the energy of an allowed electronic transition of the system.[1–3] Namely, resonance Raman spectroscopy (RRS) enables to selectively isolate vibrational contributions arising from differen chromophores, providing detailed information with structural resolution also in low cross section or low concentration compounds.

In this respect, heme-proteins represent one of the most relevant examples. They are characterized by two main

visible absorption bands associated with $\pi - \pi^*$ transitions, namely, the Q band (~550 nm) and the Soret band (~400 nm). Exploiting the resonance enhancement allowed for detailed studies on the structural arrangement of these proteins, as testified by seminal works where the Raman modes have been correlated to specific nuclear motions.[4, 5] Different aspects influence how the resonance enhancement depends on the photon wavelength, related to both the vibrational mode frequency[6–8] and to the electronic resonance.[7, 9, 10] The structural characterization has allowed to investigate ligation, oxidation, porphyrin core size, spin state of the central metal atom,[3] exploiting isotope substitution,[11] point mutations,[12] cryogenic conditions,[13] dependence on solvent pH,[14] and composition.[15]

Moreover, the aim to understand the different processes that modulate the specific function of heme-proteins, such as the mechanisms ruling ligand binding and allosteric regulation, has motivated great efforts towards time-resolved studies. In fact, both ligand photolysis and thermal relaxation in the heme moiety take place over ultrashort timescales, from fractions to tens of picoseconds. Down to a few picoseconds, the vibrational evolution can be tracked by single pulse techniques as transient Resonance Raman Scattering[16] and pump-probe experiments as in time-resolved resonant Raman.[17, 18] These methods, however, become ineffective in the exploration of subpicosecond temporal realms,[19, 20] due to the fundamental restrictions dictated by the Fourier transform limit.

Recently, the development of nonlinear optics has allowed to conceive new vibrational spectroscopies based on pulsed lasers.[20–25] In particular, broadband stimulated Raman spectroscopy (SRS)[26–28] interrogates the sample through the joint action of a pair of overlapped Raman pulse (RP) and probe pulse (PP) at different wavelengths. When the difference of their wavelengths equals a Raman active mode, the SRS effect modifies the intensity and the spectral profile of the detected PP, providing high intensity coherent signals. For instance, this technique is intensively used in microscopy to select different species in a label-free configuration.[29] Notably, the probed Raman features are engraved onto the highly directional PP, and hence, SRS provides an efficient suppression of the incoherent fluorescence background, which, on the contrary, often plagues RRS spectroscopies overwhelming the Raman signatures. SRS is a heterodyne detected technique, ie, the Raman signal is retrieved as a gain on the top of the PP spectral profile, at odds with the SR homodyne detection. Therefore, although in SR the radiation–matter interaction generates new spectral components (positive peaks) emerging over the dark noise, the SRS gain can result in more complex profiles, with positive or negative amplitudes. In particular, the SRS components that are blueshifted with respect to the RP have no spontaneous anti-Stokes Raman counterpart,[30] with profiles evolving from negative losses to positive gains through dispersive lineshapes as a function of the resonance condition.[31, 32] On the contrary, the redshifted SRS signal typically shows positive profiles analogous to the Stokes bands detected in SR. Moreover, in SR spectroscopy, the red and blue sides of the spectrum correspond to Stokes and anti-Stokes processes, respectively. Importantly, this is not the case for SRS: the SRS red-blue side ratio is indeed insensitive to the local temperature.[30] For these reasons, in order to provide a direct comparison of spontaneous and stimulated Raman techniques, in the next sections we will focus only on the red side of the SRS spectrum.

In our experiments, the narrowband RP has a 3-ps time duration and the femtosecond PP extends over the 400 to 700-nm region. After the SRS interaction, the PP pulse containing the Raman gain is dispersed onto an optical multichannel analyzer. Such a pulse scheme has several important advantages: (a) a simultaneous detection of the whole vibrational manifold, (b) a spectral resolution comparable with SR, (c) the suppression of any fluorescence background, due to the highly directional nature of the PP, (d) the possibility to turn SRS into femtosecond SRS,[19, 26, 33–35] by simply adding an ultrashort excitation pump pulse, which triggers a photochemical process of interest. Thanks to the different temporal and spectral properties of the pulses, femtosecond SRS represents an ideal tool to study structural changes in ultrafast photophysical and photochemical processes, providing both femtosecond time precision and high spectral resolution.[28, 35–37]

Here we report the application of stimulated resonance Raman scattering (SRRS) on heme-proteins, tuning the RP at wavelengths matching the two dominant electronic transitions in the visible absorption (Soret and Q bands). In particular, we select a heme-protein model for studying the tertiary protein motions, namely, myoglobin (Mb),[38] which possesses the key elements for understanding the molecular cooperativity exhibited by hemoglobin in the transport of oxygen.

Beyond assessing the spectral equivalence with RRS, understanding the SRRS response at different electronic and vibrational resonances is of primary importance for both ultrafast[19] and imaging[39] applications.

2 | EXPERIMENT

2.1 | Experimental setup

The two beams needed for the SRRS experiment are synthesized from a Ti:sapphire laser, which generates 3.6 mJ
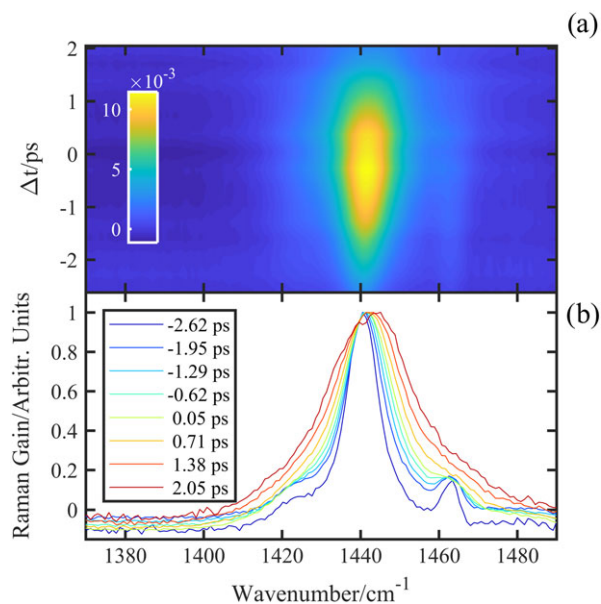
FIGURE 1 Stimulated Raman spectra at different time delays between probe pulse and Raman pulse in cyclohexane. The decrease of cross section reducing the pulses time overlap is testified by colormap (a). However, for negative time delays (ie, for a probe pulse preceding the Raman pulse) the spectral resolution increases, as emphasized by the normalized spectra in the (b) panel. In particular, for $\Delta t < -1$ ps, two close vibrational wavenumbers (1,442 and 1,464 cm^{-1}) can be distinguished

of 40 fs pulses at 800 nm with 1 kHz of repetition rate. The femtosecond PP is a white-light continuum obtained by focusing a small portion of the laser fundamental into a sapphire crystal. The generation of a narrowband RP is the key point for obtaining stimulated Raman spectra with high-frequency resolution finely tunable across an arbitrary electronic resonance. In our case, the RP is synthesized from a two-stage optical parametric amplifier (OPA) that produces tunable near-infrared pulses, followed by a spectral compression stage based on frequency doubling in a 25-mm-beta barium borate crystal.[40] An additional cleaning of the spectral frequency is performed by a double-pass (2f) spectral filter, which enables at the same time to reduce the pulse linewidth and to increase its time duration (as expected by Fourier transform limit), rectifying its temporal profile.[41, 42] RP with central wavelengths of 557 nm, ~15 cm^{-1} of bandwidth, and 439.5 nm, with a width of ~10 cm^{-1}, have been used for measuring SRRS spectra in resonance with the Q and Soret bands, respectively. For both the resonance conditions, the RP energy has been set at 600 nJ. Both pulses were linearly polarized, with parallel PP and RP fields. The two pulses were focused noncollinearly (~10°) on the sample. The PP is frequency dispersed by a spectrometer onto a Charge-Coupled Device device, able to perform single-shot acquisitions. A synchronized chopper blocks

alternating RPs in order to obtain the Raman gain using successive PPs. Indicating the PP spectrum with and without the presence of the RP as $I_P(\omega)$ and $I_P^{(0)}(\omega)$, the Raman gain is obtained as $\frac{I_P(\omega)}{I_P^{(0)}(\omega)} - 1$.

Notably, the time delay Δt between the two pulses plays a crucial role in determining intensities and lineshapes of SRRS spectral features. As experimentally shown in Figure 1a for liquid cyclohexane, the signal is enhanced when the arrival time of the PP slightly precedes the RP. On the other hand, the spectral resolution increases as Δt decreases. This effect can be rationalized by considering the nonlinear nature of the SRS signal, generated by three light–matter interactions.[21] After being stimulated by the simultaneous presence of RP and PP, the oscillating vibrational coherence dephases with its characteristic time until a third interaction with the RP gates it, leading to the signal emission. The effective time window in which the vibrational coherence evolves, and hence the effective spectral resolution of a SRS experiment, is defined by the residual duration of the RP after the coherence generation. For this reason, the spectral resolution keeps increasing as the effective window is extended, or equivalently as Δt decreases, reducing the gating of the vibrational coherence. On the other hand, the intensity of the SRS peaks is affected by two concurring terms: the amplitude of the RP at the PP arrival time and the length of the effective time window.[43] Due to these two competing factors, the maximum signal intensity appears at
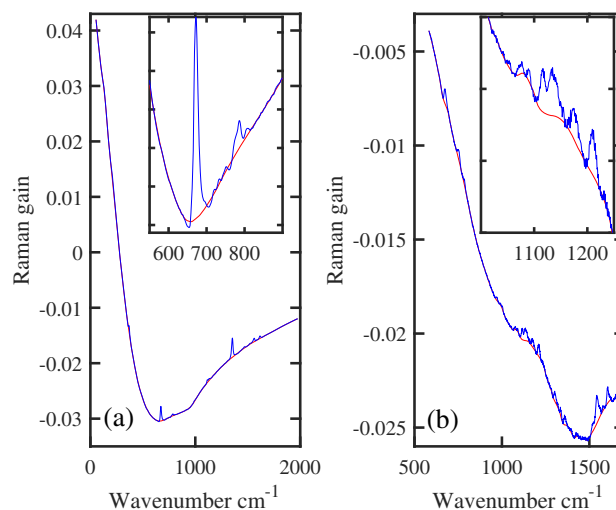
FIGURE 2 Raman gain of stimulated resonance Raman scattering experiment in deoxy myoglobin tuning the Raman pulse wavelength to match the Soret (a) and the Q bands (b). As opposed to the nonresonant cyclohexane stimulated Raman spectroscopy measurement shown in Figure 1, myoglobin spectra are accompanied by Raman pulse-induced absorption changes of the probe pulse, which we remove through a baseline subtraction routine, as detailed in the main text. The baselines, obtained by a smoothing algorithm, are represented by red lines

slightly negative time delays. For these reasons, a mechanical delay line is used to scan Δt, in order to optimize the trade-off between the spectral resolution and peak intensity.

2.2 | Sample preparation

Horse heart Mb was purchased from Sigma-Aldrich. The freeze-dried protein was dissolved in degassed 0.1 M phosphate buffer (pH 7.5), initially in the Fe(III) oxidation state ("ferric" Mb), which is the stable air-exposed form. The Mb solution was prepared anaerobically in a transmission cell under a pure nitrogen atmosphere to prevent exposure to atmospheric oxygen. A sodium dithionite solution was added to reduce the heme group to the Fe(II) oxidation state ("deoxy form"). The sample was allowed to flow anaerobically through the transmission cell during the experiment by means of a peristaltic pump, so as to guarantee a fresh sample at every laser shot (1 KHz). The thickness of the sample was 0.5 mm, and the concentration was 150 μM and 1.6 mM for the measurement at Soret band and at Q band, respectively. All the Raman measurements were performed at room temperature.

3 | RESULTS AND DISCUSSION

The results of SRRS measurements on deoxy Mb in the Soret and Q bands are reported in Figure 2 as blue lines. Critically, transmission changes induced by the RP portion that precedes the short PP and additional nonlinear contri-

butions from both the solvent and the Mb can lead to broad background signals. For this reason, the SRRS gain usually appears on the top of a baseline, which has to be further removed in order to isolate the Raman contributions. Considering the richer frequency dependence of the Raman signatures with respect to that of the background,[44–46] we can extract the corrected SRRS spectrum dividing the Raman gain by an iterative spline interpolation performed on the data.[47] As a first step, the spline is performed on the full spectral range, and the regions that deviate from it up to a positive fixed threshold are defined as those influenced by Raman effects. Then, a similar spline process is iteratively applied to the spectral regions marked as non-Raman in the previous step, and an analogous procedure is used to identify the region that has to be excluded in the next step. The baseline that has been removed from the data, shown by the red lines in Figure 2, has been obtained iterating 4 times the spline procedure.

The resulting SRRS spectra of deoxy Mb in resonance with the Soret band are reported by the red lines in Figure 3. The narrowband ($\sim$10 cm^{-1}) nature of RP guarantees a spectral resolution analogous to that of the RRS measurements from previous works.[3, 12] We find a very good agreement between the peak positions in our data and the vibrational wavenumbers reported in literature. Specifically, we observe a dominant contribution of ν_4 and ν_7 modes, which exhibit the A_{1g} symmetry.[4] As shown in Figure 4, by tuning the RP at 557 nm, we probe the Q band-resonant SRRS spectrum. In analogy with the RRS measurements, performed under similar resonance conditions,[9] peak intensities are affected by the change in RP wavelength. In particular, a large
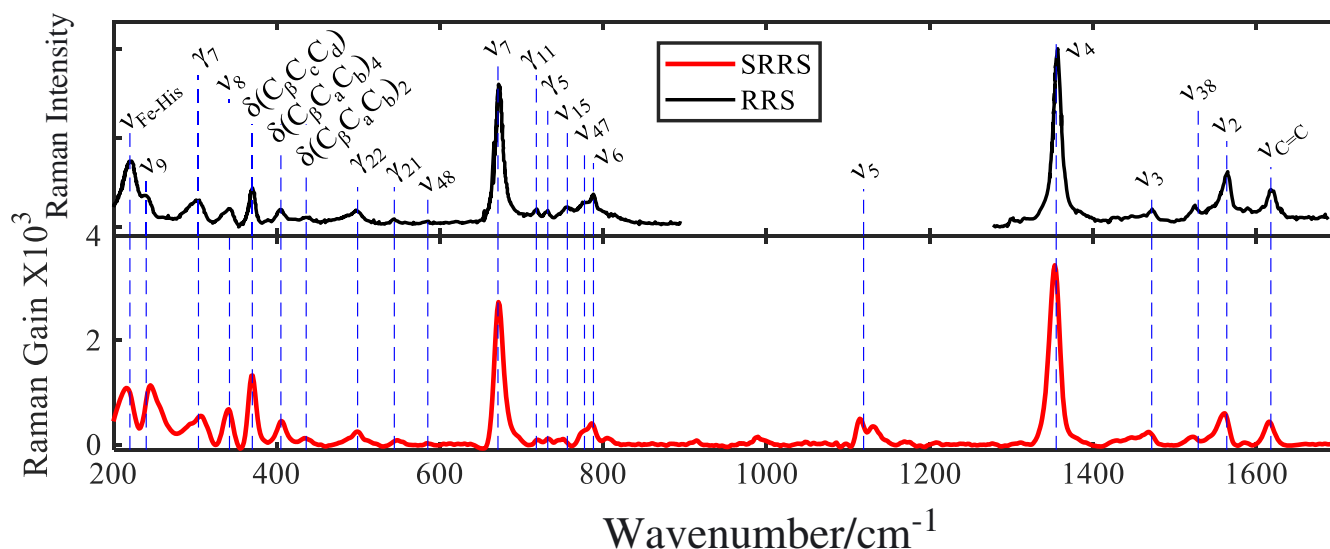
FIGURE 3 Stimulated resonance Raman scattering (SRRS) spectra obtained with the Raman pulse at 439.5 nm (red line). The SRRS bands are compared to those obtained by resonance Raman spectroscopy (RRS) at 441.7 nm in the low[12] and high[3] wavenumber range (black lines). The most intense bands are highlighted by blue dashed lines and labeled by Abe notation
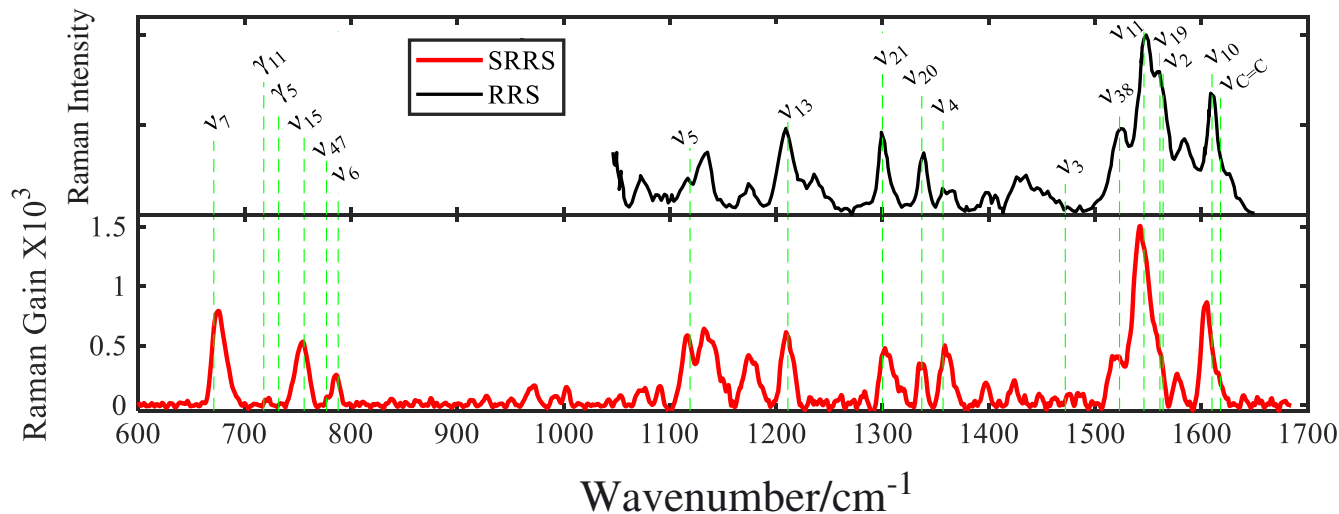
FIGURE 4 Stimulated resonance Raman scattering (SRRS) spectra obtained with the Raman pulse at 557 nm (red line). The SRRS result is compared to those obtained by resonance Raman spectroscopy (RRS) at 565 nm reported in Franzen et al.[9] (black line). The most intense bands are highlighted by green dashed lines and labeled with Abe notation

cross section enhancement of the modes with B_{1g} and A_{2g} symmetry (ν_{10-28}) is revealed, whereas modes with A_{1g} symmetry (as ν_3, ν_4, and ν_5) appear less intense. As sketched in Figure 5, in the Raman processes, the excitations of vibrational coherences are sensitive to the mode-specific coupling to the electronic transition that makes different vibrational modes undergoing diverse resonance enhancements.[9, 10, 48, 49]

For both the probed resonance conditions, the SRRS spectra show a general agreement with the RRS data. The latter are reported as black lines in Figures 3 and 4, for the spectral regions available in the literature.[3, 9, 12] A careful inspection of the Raman shifts and mode intensities (extracted as the area of fitted Lorentzian profiles and reported in Table 1) reveals significant deviations in the relative amplitudes and small shifts in the peak positions.

In SR spectroscopy, the emitted radiation is typically collected at 90° with respect to the pump pulse, without selecting any polarization component. Measuring the emitted Raman photons with polarizations only parallel ($I_{//}$) or orthogonal ($I_{\perp}$) to a vertically polarized PP can be exploited to measure the depolarization ratio $\rho = \frac{I_{\perp}}{I_{//}}$.[50] In our SRRS experiments, performed in forward collection, only the photons with polarization parallel to the PP undergo stimulated Raman effect. Therefore, when the PP and RP have parallel polarizations, the SRRS signal corresponds to the $I_{//}$ intensity detected in an SR experiment. For this reason, a direct comparison of the peak amplitudes should take into account the depolarization ratio ρ, with the intensity ratio of the SR and SRRS amplitudes scaling as $\frac{I_{RRS}}{I_{SRRS}} = 1 + \rho$. In Table 1,

the validity of such a scaling is verified, using depolarization ratios measured in Bangcharoenpaurpong et al.[6] and Franzen et al.[9] Significant deviation of $\frac{1+\rho}{I_{RRS}/I_{SRRS}}$ from unity are found, as reported in Table 1, likely induced by the slightly different RP wavelengths of RRS and SRRS experiments (441.7 and 565 nm for the RRS and 439.5 and 557 nm for the SRRS, for Soret and Q band-resonant Raman spectra, respectively) and ρ extrapolation, measured at 568 and 434 nm. Both ρ and the Raman peak cross section depend indeed on the RP wavelength across the absorption profile.[49]

The similarity between spontaneous and stimulated Raman spectra can be rationalized evaluating the optical signals through perturbative expansion of the polarization in powers of the radiation–matter interaction Hamiltonian.[21, 51] The use of a diagrammatic framework, developed to represent in a compact way different nonlinear optical processes,[52] shows that both spontaneous and stimulated Raman scattering arise from the third-order nonlinear susceptibility $\chi^{(3)}$.[21] Under nonresonant conditions, it is well established that SR and SRS signals can be expressed as a function of the same $\chi^{(3)}$ [22] and they are accounted for by the same terms in the diagrammatic theory.[53] For this reason, the SRS spectrum, in the region redshifted with respect to the narrowband RP, gives the same information of its spontaneous counterpart,[31, 41, 54] albeit that the two effects are generated through different radiative processes. On the contrary, when the RP is tuned in resonance with an electronic transition, besides intensity enhancements, spectral features in SRRS possibly experience lineshape modifications due to the specific conditions in which the experiment is done (mismatch from

TABLE 1 Mode assignment, peak positions, intensities, and depolarization ratios (ρ) for Raman-active modes in deoxy myoglobin recorded under Soret and Q bands resonant excitations. Dashes indicate that the corresponding Raman band has not been observed in the measurements.

	Soret						Q band					
Mode	ν_{SRRS} (cm^{-1})	ν_{RRS} (cm^{-1})	I_{SRRS}	I_{RRS}	ρ	$\frac{1+\rho}{I_{RRS}/I_{SRRS}}$	ν_{SRRS} (cm^{-1})	ν_{RRS} (cm^{-1})	I_{SRRS}	I_{RRS}	ρ	$\frac{1+\rho}{I_{RRS}/I_{SRRS}}$
ν_{Fe-His}	213	220	8.1	14.7	0.15	0.6						
ν_9	247	242	8.4	1.1								
γ_7	298	300	7.2	4.8								
ν_8	341	339	2.7	1.3								
$\delta(C_\beta C_c C_d)$	370	370	5.0	2.8	0.13	2.0						
$\delta(C_\beta C_a C_b)_4$	405	405	2.8	1.4								
$\delta(C_\beta C_a C_b)_2$	435	435	1.1	1.0								
—	490	482	2.0	1.4								
γ_{22}	499	498	1.1	1.7								
γ_{21}	550	544	0.8	0.3								
ν_7	672	673	12.9	15.0	0.16	1.0	676		8.1			
γ_{11}	721	717	0.5	0.9			-		-			
γ_5	734	731	0.4	0.8			-		-			
ν_{15}	749	755	0.7	2.1			754		5.2			
ν_{47}	774	777	1.1	3.0			-		-			
ν_6	786	788	1.5	1.1			786		1.5			
—	-	806		1.2			-		-			
—	-	-	-				971		1.2			
ν_5	1,115		1.9				1,115	1,114	3.6	3.4		
—	1,133		2.3				1,135	1,133	9.8	5.4		
—	-		-				1,176	1,175	4.7	1.3	0.42	5.2
ν_{13}	-		-				1,210	1,209	5.4	8.8	0.48	0.9
ν_{21}	-	-	-	-			1,305	1,300	4.9	5.2	1.41	2.2
ν_{20}	-	-	-	-			1,337	1,338	2.2	3.4	0.77	1.1
ν_4	1,353	1,357	17.5	20.5	0.17	1.0	1360	1363	4.1	1.6	0.37	3.5
—	-	-	-	-			1,397	1,398	1.0	0.8	0.64	1.9
—	-	-	-	-			-	-	-	-	0.65	
—	1,428	1,427	1.1	0.6			1,424	1,431	1.1	4.2		
—	1,446	1,455	0.5	3.1			-	-	-	-		
ν_3	1,467	1,473	2.2	0.9			-	-	-	-	0.24	
ν_{38}	1,520	1,525	1.3	1.5			1,518	1,522	3.6	5.5	0.61	1.0
ν_{11}	1,550	1,556	1.9	6.0			1,544	1,548	20.6	24.1	0.81	1.5
ν_{19}	1,561	1,565	2.2	3.9			1,561	1,563	1.2	3.9	1.00	0.6
—	1,587	1,591	0.5	1.3			1,578	1,584	1.5	5.1	0.52	0.5
ν_{10}	-	-	-	-			1,604	1,610	6.3	9.3	0.47	1.0
ν_{C-C}	1,616	1,620	2.6	6.1			1,616	1,627	1.6	1.2		

Note. The stimulated resonance Raman scattering (SRRS) spectra are compared with resonance Raman spectroscopy (RRS) results extracted from the spectra in Spiro[3], Franzen et al.[9], and Hu et al.[12], and the intensities have been estimated as the area of the specific Raman bands. The RRS reported in Figures 3 and 4 have been normalized at the intensity of the ν_{10}, ν_7, and ν_4 modes, for the Q band-resonant and low and high wavenumber region Soret band-resonant spectra, respectively. The ratio $\frac{1+\rho}{I_{RRS}/I_{SRRS}}$ reported in the table has been calculated using the depolarization ratio ρ reported in Bangcharoenpaurpong et al.[6] for the Soret band and in Franzen et al.[9] for the Q band.

the "full" resonant wavelength, shape of the absorption spectrum, Condon factors, vibronic coupling, or multimode effects) and to additional diagrams, representing different matter–fields interactions with no spontaneous analogues. Notably, although the specific dependence of the SRRS blue side lineshapes on the RP wavelength and absorption spectrum has been recently addressed,[55–57] the nature of the spectral profiles in the red side of an SRRS spectrum is currently debated.[44, 57–59] In particular, the presence of peak shifts and dispersive shapes under
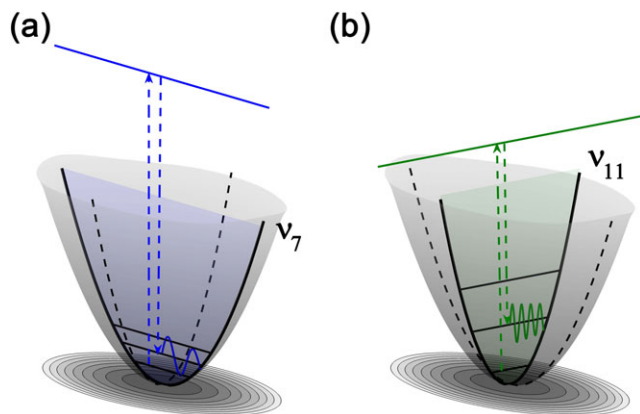
FIGURE 5 Concept of resonant Raman enhancement under distinct electronic excitations in deoxy myoglobin. The ν_7 band is coupled to the Soret electronic transition, and hence, efficient coherent stimulation of this mode is achieved by the joint action of a ~440 nm Raman pulse and a redshifted probe pulse. On the contrary, the ν_{11} is electronically coupled to the Q band, and hence, it undergoes a resonant enhancement upon an excitation with a Raman pulse tuned at ~540 nm

specific electronic resonances has been advanced.[31] In our SRRS measurements, performed in resonance with the two different broad electronic levels in the visible range of Mb, no dispersive features have been observed. These observations hence indicate that SRRS is a powerful tool to extract the Raman excitation profiles in heme-proteins, which can be directly compared to the ones obtained by continuous-wave RRS measurements.

4 | CONCLUSIONS

Using a narrowband (10–15 cm^{-1} of bandwidth), frequency tunable RP, we measured the SRRS spectra of deoxy Mb, in resonance with the two main absorption bands in the visible, the Q and Soret bands. We found an excellent agreement between our measurements and SR data, achieving at the same time an efficient suppression of fluorescence background.

In the last years, spectral profiles of SRS bands upon resonant conditions have been the focus of an intense debate. Lineshape modifications, such as dispersive or broad profiles, can potentially hamper the spectral interpretation. On the basis of the present observations and on Ferrante et al.[19] and Batignani et al.,[57] this seems not to be the case in Mb, for which sharply positively peaked SRRS features have been reported. A crucial advantage of the presented SRS experiment is represented by the possibility of continuously tuning the RP wavelength,[40] allowing a fine mapping of the Raman excitation profiles along the sample absorption bands, as recently shown in Batignani et al.[57]

Our results substantiate the potential of this technique as a competitive candidate for the vibrational characterization of complex macromolecules. Moreover, the extension of SRS to the domains of microscopy[29] and time-resolved studies[19, 47, 60] boosts its significance as a state-of-the-art spectroscopic tool for the biochemical and material sciences.

ORCID

T. Scopigno http://orcid.org/0000-0002-7437-4262

REFERENCES

[1] D. P. Strommen, K. Nakamoto, *J. Chem. Educ.* **1977**, *54*, 474.

[2] T. G. Spiro, *Proc. R. Soc. A* **1975**, *345*, 89.

[3] T. G. Spiro, *Biological Applications of Raman Spectroscopy: Resonance Raman Spectra of Haeme and Metalloproteins*, *Vol. 3*, John Wiley & Sons, New York **1988**.

[4] M. Abe, T. Kitagawa, Y. Kyogoku, *J. Chem. Phys.* **1978**, *69*, 4526.

[5] X. Y. Li, R. S. Czernuszewicz, J. R. Kincaid, Y. O. Su, T. G. Spiro, *J. Phys. Chem.* **1990**, *94*, 31.

[6] O. Bangcharoenpaurpong, K. T. Schomacker, P. M. Champion, *J. Am. Chem. Soc.* **1984**, *106*, 5688.

[7] B. R. Stallard, P. R. Callis, P. M. Champion, A. C. Albrecht, *J. Chem. Phys.* **1984**, *80*, 70.

[8] T. C. Strekas, T. G. Spiro, *J. Raman Spectrosc.* **1973**, *1*, 387.

[9] S. Franzen, S. E. Wallace-Williams, A. P. Shreve, *JACS* **2002**, *124*, 7146.

[10] J. A. Shelnutt, *The J. Chem. Phys.* **1981**, *74*, 6644.

[11] M. Tsubaki, N. T. Yu, *Biochemistry* **1982**, *21*, 1140.

[12] S. Hu, K. M. Smith, T. G. Spiro, *JACS* **1996**, *118*, 12638.

[13] M. R. Ondrias, D. L. Rousseau, S. R. Simon, *J. Biol. Chem.* **1983**, *258*, 5638.

[14] G. Smulevich, J. M. Mauro, L. A. Fishel, A. M. English, J. Kraut, T. G. Spiro, *Biochemistry* **1988**, *27*, 5477.

[15] J. Teraoka, T. Kitagawa, *J. Biol. Chem.* **1981**, *256*, 3969.

[16] J. J. Loparo, C. M. Cheatum, M. R. Ondrias, M. C. Simpson, *Chem. Phys.* **2003**, *286*, 353.

[17] Y. Mizutani, *Science* **1997**, *278*, 443.

[18] S. Franzen, B. Bohn, C. Poyart, J. L. Martin, *Biochemistry* **1995**, *34*, 1224.

[19] C. Ferrante, E. Pontecorvo, G. Cerullo, M. H. Vos, T. Scopigno, *Nat Chem* **2016**, *8*, 1137.

[20] A. H. Zewail, *J. Phys. Chem. A* **2000**, *104*, 5660.

[21] S Mukamel, *Principles of Nonlinear Optical Spectroscopy*, Oxford University Press, New York **1995**.

[22] *Coherent Raman Scattering Microscopy (Series in Cellular and Clinical Imaging)* (Eds:J. X. Cheng, X. S. Xie), CRC Press, London **2016**.

[23] E. Ploetz, S. Laimgruber, S. Berner, W. Zinth, P. Gilch, *Appl. Phys. B* **2007**, *87*, 389.

[24] M. Kowalewski, K. Bennett, K. E. Dorfman, S. Mukamel, *Phys. Rev. Lett.* **2015**, *115*, 193003.

[25] L. Monacelli, G. Batignani, G. Fumero, C. Ferrante, S. Mukamel, T. Scopigno, *J. Phys. Chem. Lett.* **2017**, *8*, 966.

[26] M. Yoshizawa, Y. Hattori, T. Kobayashi, *Phys. Rev. B* **1994**, *49*, 13259.

[27] D. W. McCamant, P. Kukura, S. Yoon, R. A. Mathies, *Rev. Sci. Instrum.* **2004**, *75*, 4971.

[28] P. Kukura, D. W. McCamant, R. A. Mathies, *Annu. Rev. Phys. Chem.* **2007**, *58*, 461.

[29] C. W. Freudiger, W. Min, B. G. Saar, S. Lu, G. R. Holtom, C. He, J. C. Tsai, J. X. Kang, X. S. Xie, *Science* **2008**, *322*, 1857.

[30] U. Harbola, S. Umapathy, S. Mukamel, *Phys. Rev. A* **2013**, *88*, 011801(R).

[31] R. R. Frontiera, S. Shim, R. A. Mathies, *J. Chem. Phys.* **2008**, *129*, 064507.

[32] B. Mallick, A. Lakhsmanna, S. Umapathy, *J. Raman Spectrosc.* **2011**, *42*, 1883.

[33] P. Kukura, D. W. McCamant, S. Yoon, D. B. Wandschneider, R. A. Mathies, *Science* **2005**, *310*, 1006.

[34] G. Batignani, D. Bossini, N. Di Palo, C. Ferrante, E. Pontecorvo, G. Cerullo, A. Kimel, T. Scopigno, *Nature Photon.* **2015**, *9*, 506.

[35] D. R. Dietze, R. A. Mathies, *ChemPhysChem* **2016**, *17*, 1224.

[36] S. Mukamel, J. D. Biggs, *J. Chem. Phys.* **2011**, *134*, 161101.

[37] G. Fumero, G. Batignani, K. E. Dorfman, S. Mukamel, T. Scopigno, *Chem. Phys. Chem.* **2015**, *16*, 3438.

[38] M. Brunori, *Protein Science* **2010**, *19*, 195.

[39] D. Zhang, M. N. Slipchenko, D. E. Leaird, A. M. Weiner, J. X. Cheng, *Opt. Express* **2013**, *21*, 13864.

[40] E. Pontecorvo, S. M. Kapetanaki, M. Badioli, D. Brida, M. Marangoni, G. Cerullo, T. Scopigno, *Opt. Express* **2011**, *19*, 1107.

[41] E. Pontecorvo, C. Ferrante, C. G. Elles, T. Scopigno, *Opt. Express* **2013**, *21*, 6866.

[42] D. P. Hoffman, D. Valley, S. R. Ellis, M. Creelman, R. A. Mathies, *Opt. Express* **2013**, *21*, 21685.

[43] S. Yoon, D. W. McCamant, P. Kukura, R. A. Mathies, D. Zhang, S. Y. Lee, *J. Chem. Phys* **2005**, *122*, 024505.

[44] A. Weigel, A. Dobryakov, B. Klaumünzer, M. Sajadi, P. Saalfrank, N. P. Ernsting, *J. Phys. Chem. B* **2011**, *115*, 3656.

[45] S. Laimgruber, H. Schachenmayr, B. Schmidt, W. Zinth, P. Gilch, *Appl. Phys. B* **2006**, *85*, 557.

[46] M. Kloz, R. van Grondelle, J. T. M. Kennis, *Chem. Phys. Lett.* **2012**, *544*, 94.

[47] E. Pontecorvo, C. Ferrante, C. G. Elles, T. Scopigno, *J. Phys. Chem. B* **2014**, *118*, 6915.

[48] J. A. Shelnutt, L. D. Cheung, R. C. C. Chang, N. T. Yu, R. H. Felton, *J. Chem. Phys.* **1977**, *66*, 3387.

[49] D. W. Collins, P. M. Champion, D. B. Fitchen, *Chem. Phys. Lett.* **1976**, *40*, 416.

[50] D. A. Long, *The Raman Effect: A Unified Treatment of the Theory of Raman Scattering by Molecules*, Wiley, Chichester; New York **2002**.

[51] G. Batignani, G. Fumero, S. Mukamel, T. Scopigno, *Phys. Chem. Chem. Phys.* **2015**, *17*, 10454.

[52] J. D. Biggs, J. A. Voll, S. Mukamel, *Phil. Trans. R. Soc. A* **2012**, *370*, 3709.

[53] Z. Sun, J. Lu, D. H. Zhang, S. Y. Lee, *J. Chem. Phys.* **2008**, *128*, 144114.

[54] E. C. Ploetz, M. Gellner, M. Schütz, B. Marx, S. Schlücker, P. Gilch, *AIP Conf. Proc.* **2010**, *1267*, 88.

[55] S. Umapathy, B. Mallick, A. Lakshmanna, *J. Chem. Phys.* **2010**, *133*, 024505.

[56] Q. Cen, Y. He, M. Xu, J. Wang, Z. Wang, *J. Chem. Phys.* **2015**, *142*, 114201.

[57] G. Batignani, E. Pontecorvo, G. Giovannetti, C. Ferrante, G. Fumero, T. Scopigno, *Sci. Rep.* **2016**, *6*, 18445.

[58] B. Zhao, K. Niu, X. Li, S. Y. Lee, *Sci. China Chem.* **2011**, *54*, 1989.

[59] S. Shim, C. M. Stuart, R. A. Mathies, *Chem. Phys. Chem.* **2008**, *9*, 697.

[60] G. Batignani, E. Pontecorvo, C. Ferrante, M. Aschi, C. G. Elles, T. Scopigno, *J. Phys. Chem. Lett.* **2016**, *7*, 2981.